



HAL
open science

The inherent strain method for additive manufacturing: critical analysis and new inherent strain rate method

Michel Bellet, Joël Keumo Tematio, Y Zhang

► To cite this version:

Michel Bellet, Joël Keumo Tematio, Y Zhang. The inherent strain method for additive manufacturing: critical analysis and new inherent strain rate method. MCWASP XVI, 16th Int. Conf. on Modeling of Casting, Welding and Advanced Solidification Processes, Jun 2023, Banff (Alberta), Canada. pp.012001, 10.1088/1757-899x/1281/1/012001 . hal-04491793

HAL Id: hal-04491793

<https://minesparis-psl.hal.science/hal-04491793>

Submitted on 6 Mar 2024

HAL is a multi-disciplinary open access archive for the deposit and dissemination of scientific research documents, whether they are published or not. The documents may come from teaching and research institutions in France or abroad, or from public or private research centers.

L'archive ouverte pluridisciplinaire **HAL**, est destinée au dépôt et à la diffusion de documents scientifiques de niveau recherche, publiés ou non, émanant des établissements d'enseignement et de recherche français ou étrangers, des laboratoires publics ou privés.

PAPER • OPEN ACCESS

The inherent strain method for additive manufacturing: critical analysis and new inherent strain rate method

To cite this article: M Bellet *et al* 2023 *IOP Conf. Ser.: Mater. Sci. Eng.* **1281** 012001

View the [article online](#) for updates and enhancements.

You may also like

- [Standing Sausage Perturbations in Solar Coronal Slabs with Continuous Transverse Density Profiles: Cutoff Wavenumbers, Evanescent Eigenmodes, and Oscillatory Continuum](#)
Zexing Wang, Bo Li, Shao-Xia Chen et al.
- [Development of a vascular substitute produced by weaving yarn made from human amniotic membrane](#)
Agathe Grémare, Lisa Thibes, Maude Gluais et al.
- [Current biofabrication methods for vascular tissue engineering and an introduction to biological textiles](#)
Fabien Kawecki and Nicolas L'Heureux



Connect with decision-makers at ECS

Accelerate sales with ECS exhibits, sponsorships, and advertising!

▶ Learn more and engage at the 244th ECS Meeting!

The inherent strain method for additive manufacturing: critical analysis and new inherent strain rate method

M Bellet, J Keumo Tematio, Y Zhang

Mines Paris, PSL University, CEMEF – Centre de Mise en Forme des Matériaux, CNRS UMR 7635, Sophia Antipolis, France. Email: michel.bellet@minesparis.psl.eu

Abstract. To reduce computation time, the inherent strain (IS) method is popular. It consists in adding layers, at room temperature, with an "inherent strain" representing the plastic deformation undergone during deposition. An IS method is developed, including a direct determination of the IS tensor based on the transient thermo-elastic-viscoplastic (TEVP) simulation. Validation is achieved: taking full-field inherent strains, the IS method allows retrieving TEVP predictions. However, application to a full part, for which a set of inherent strains must be conserved all along the construction, leads to poor results, far from TEVP. As an alternative, a new "inherent strain rate" (ISR) method is proposed, consisting in linearizing TEVP resolutions. Combined with an on-line learning technique, this strategy leads to results identical to TEVP reference, with still a significant speed-up. This makes the proposed ISR method very promising.

1. Introduction

The paper focuses on thermomechanical simulation of additive manufacturing (AM), especially DED (Directed Energy Deposition). Numerical tools are strategic to optimize manufacturing routes. However, for large parts, and despite some shortcomings (fluid flow ignored in melt pool, material deposited by batch: fractions of layer, groups of several layers), simulation time remains quite long. To maintain computation time in an acceptable range, the inherent strain (IS) method, initially developed for welding simulation by Ueda *et al.* [1], was adapted to AM, first by Keller & Ploshikhin [2]. Since then, different variants of the IS method have been developed (Alvarez *et al.* [3], Liang *et al.* [4]). They differ essentially by the mode of determination of the inherent strains, which has a high impact on results. Because of that, the approach developed here consists in determining the IS in such a way that the IS method replicates the transient thermomechanical simulation. For that, we take as reference a finite element simulation developed and validated separately. This transient thermomechanically coupled simulation, based on an elastic-viscoplastic constitutive model, is not reported here, as it is not essential to the purpose of the present study. It can be found in [5], and it will be referred as STD-TEVP. Throughout the rest of the paper, we will not compare numerical predictions to experimental measurements, but to results obtained by this STD-TEVP simulation.

The paper is structured as follows. Section 2 consists of a short description of the IS method, and of the different methods to determine the inherent strains. In Section 3, the new technique to determine the IS will be presented. It consists of a direct determination based on the STD-TEVP simulation of the first layers deposition of the studied part. However, it will be shown that this method – although validated on these first layers – leads to poor results for the whole part. Therefore, in Section 4, an alternative method will be presented: the inherent strain rate method, which is based on a linearization of the reference STD-TEVP simulation. This new method leads to excellent results, in perfect agreement with the reference ones.



2. Inherent strain method

2.1. Main features, in AM context

In the IS method material addition is conducted layer-by-layer, isothermally, at room temperature, and without any time consideration. This is a huge simplification compared to the STD-TEVP approach in which the progress of the build process is simulated. In the IS method, after each layer addition, the static equilibrium of the growing structure is solved at ambient temperature, by performing a finite element (FE) resolution of the weak form of the vector equation:

$$\nabla \cdot \boldsymbol{\sigma} + \rho \mathbf{g} = 0 \quad (1)$$

where $\boldsymbol{\sigma}$ is the stress tensor, ρ the density, and \mathbf{g} the gravity vector. Owing to the hypotheses made on temperature and time, and to the small deformation context of AM, the behavior law is of elastic-plastic type, with isotropic hardening (for extension to kinematic hardening, refer to Keumo Tematio [5]):

$$\boldsymbol{\varepsilon} = \boldsymbol{\varepsilon}^{el} + \boldsymbol{\varepsilon}^{pl} + \boldsymbol{\varepsilon}^* \quad \boldsymbol{\varepsilon}^{el} = \mathbf{S}^{el} \boldsymbol{\sigma} \quad \left\{ \begin{array}{l} \bar{\sigma} < \sigma_Y + R(\bar{\varepsilon}) \quad \text{and} \quad d\boldsymbol{\varepsilon}^{pl} = 0 \\ \text{or} \quad \bar{\sigma} = \sigma_Y + R(\bar{\varepsilon}) \quad \text{and} \quad d\boldsymbol{\varepsilon}^{pl} = \frac{3d\bar{\varepsilon}}{2\bar{\sigma}} \mathbf{s} \end{array} \right. \quad (2)$$

where $\boldsymbol{\varepsilon}$ is the strain tensor, $\boldsymbol{\varepsilon}^{el}$ and $\boldsymbol{\varepsilon}^{pl}$ its elastic and plastic parts, respectively. \mathbf{S}^{el} is the elastic compliance tensor, $d\bar{\varepsilon}$ is the generalized strain increment, and $\bar{\sigma}$ is the generalized (von Mises) stress:

$$d\bar{\varepsilon} = \sqrt{(2/3)d\boldsymbol{\varepsilon}^{pl} : d\boldsymbol{\varepsilon}^{pl}} \quad \bar{\sigma} = \sqrt{(3/2)\mathbf{s} : \mathbf{s}} \quad (3)$$

where σ_Y is the initial plastic yield stress, and R is the strain hardening function. In Eq. (2) $\boldsymbol{\varepsilon}^*$ denotes the inherent strain tensor, which represents the permanent strains undergone by the deposited material. It is assigned to each newly deposited layer and is kept as such until the end of the simulation. For a part made of N layers, the IS resolution simply consists of a series of N FE resolutions of Eq. (1).

2.2. Determination of inherent strains

The key point of the IS method lies in the identification of the inherent strain tensor $\boldsymbol{\varepsilon}^*$. In the literature, essentially two ways can be found to determine $\boldsymbol{\varepsilon}^*$.

2.2.1. Comparison experiment/simulation on test specimen. A small-scale specimen is supposed to be representative of the process, e.g. a straight wall of a few superimposed tracks for DED. $\boldsymbol{\varepsilon}^*$ can be estimated by minimizing the difference between measurements and numerical simulation by IS method:

$$\boldsymbol{\varepsilon}^* = \operatorname{argmin} \left\| \mathbf{u}^{sim}(\boldsymbol{\varepsilon}^*) - \mathbf{u}^{exp} \right\| \quad (4)$$

where \mathbf{u}^{exp} denotes a set of distortion measurements, while \mathbf{u}^{sim} denotes the corresponding predictions by IS simulation. This method was used by Setien *et al.* [6], Siewert *et al.* [7], and many others.

2.2.2. Identification by simulation only of a test specimen. A small-scale specimen is considered, for which material deposition is simulated by a transient thermo-mechanical simulation, formerly validated. This allows determining some rules to estimate $\boldsymbol{\varepsilon}^*$. For instance, Liang *et al.* [4] suggested:

$$\boldsymbol{\varepsilon}^* = \boldsymbol{\varepsilon}_i^{el} + \boldsymbol{\varepsilon}_i^{pl} - \boldsymbol{\varepsilon}_s^{el} \quad (5)$$

where $\boldsymbol{\varepsilon}_i^{el}$ and $\boldsymbol{\varepsilon}_i^{pl}$ respectively stand for the calculated elastic and plastic strain tensors in a so-called intermediate state, while $\boldsymbol{\varepsilon}_s^{el}$ stands for the calculated elastic strain tensor after final cooling. The intermediate state is "the state when the heat source just passes by and the local (compressive) mechanical strain reaches the largest amplitude". This method, known as the "modified inherent strain method", has been used to simulate DED (Duan *et al.* [8]) and L-PBF processes [4]. In this framework, the three tensors at the right-hand side of Eq. (5) are directly deduced from the transient thermo-mechanical simulation. Note that contrary to the previous method – where a unique IS tensor $\boldsymbol{\varepsilon}^*$ is determined – here the IS tensor is determined everywhere, in all layers of the test specimen. This brings up the question of selecting one or two layers and averaging $\boldsymbol{\varepsilon}^*$ therein to come down to a unique tensor.

To conclude on inherent strains determination, approaches based on direct measurements appear difficult and time consuming because they require the definition and the realization of complex strain or stress measurements on test specimens. On the contrary, approaches based on thermomechanical simulation of test specimens appear more efficient, provided that the exploitation of such simulations in view of estimating the inherent strains is simple, direct, and achievable in an automatic process. In line with this last remark, a new IS method is proposed. The basic idea is to identify inherent strains such that the IS method could provide the same results as STD-TEVP on the selected test specimen. In the following Section, it will be explained how this can be achieved, by considering the inherent strain tensor as a layer-dependent and space-dependent field, the determination of which being done without any costly inverse finite element procedure, but directly and locally, based on STD-TEVP results.

3. A new inherent strain method

In this Section, prior to application to a full part, we first focus on how to determine inherent strains, based on the simulation of a small-scale test specimen with STD-TEVP formulation.

3.1. Determination of inherent strains from STD-TEVP simulations of small-scale test specimen

In the context of the DED process, the test specimen consists of a few (N) superimposed layers. Hence, N different states are defined, see Figure 1. State n is obtained after i) deposition of layers 1 to n , including inter-layer dwell times, and ii) final cooling to room temperature. In this Section, we will explain how the inherent strains can be directly and locally (in each finite element) deduced from the reference STD-TEVP simulation.

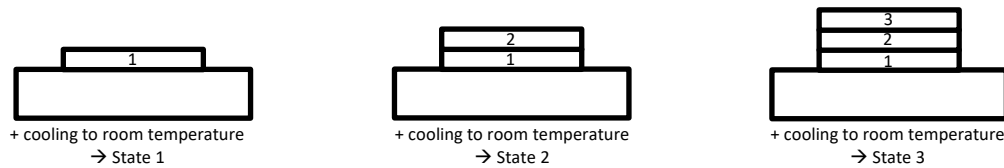


Figure 1. Schema of a small-scale 3-layer specimen, and of the three states considered.

Each of the deposition processes leading to states $1, 2, \dots, N$ is simulated by means of STD-TEVP simulation. This allows calculating, for each state n , the residual displacement and stress fields: $\mathbf{u}_{(n)}$, $\boldsymbol{\sigma}_{(n)}$ obtained after deposition of n layers and final cooling. In the context of small deformations, the differences in displacement and strain between state n and state $n - 1$ are:

$$\Delta \mathbf{u}_{(n)}^{STD} = \mathbf{u}_{(n)}^{STD} - \mathbf{u}_{(n-1)}^{STD} \quad \Delta \boldsymbol{\epsilon}_{(n)}^{STD} = (1/2) \left(\nabla(\Delta \mathbf{u}_{(n)}^{STD}) + (\nabla(\Delta \mathbf{u}_{(n)}^{STD}))^T \right) \quad (6)$$

Besides, when simulating the different states with the IS approach, we can write, from Eq. (2):

$$\Delta \boldsymbol{\epsilon}_{(n)}^{IS} = \Delta \boldsymbol{\epsilon}_{(n)}^{IS,el} + \Delta \boldsymbol{\epsilon}_{(n)}^{IS,pl} + \Delta \boldsymbol{\epsilon}_{(n)}^* \quad (7)$$

where the increment of inherent strain only affects the newly deposited layer: $\Delta \boldsymbol{\epsilon}_{(n)}^* = \mathbf{0}$ in all layers from 1 to $n - 1$. The principle leading to the identification of the inherent strains is then the following: find for each layer n the tensor $\Delta \boldsymbol{\epsilon}_{(n)}^*$ such that:

$$\Delta \boldsymbol{\epsilon}_{(n)}^{IS} = \Delta \boldsymbol{\epsilon}_{(n)}^{STD} \quad \text{and} \quad \Delta \boldsymbol{\sigma}_{(n)}^{IS} = \Delta \boldsymbol{\sigma}_{(n)}^{STD} \quad (8)$$

Taking the trace of Eq. (7), $\Delta \boldsymbol{\epsilon}_{(n)}^*$ should be such that:

$$\text{tr}(\Delta \boldsymbol{\epsilon}_{(n)}^{STD}) = \text{tr}(\Delta \boldsymbol{\epsilon}_{(n)}^{IS,el}) + \text{tr}(\Delta \boldsymbol{\epsilon}_{(n)}^*) \quad (9)$$

in which $\text{tr}(\Delta \boldsymbol{\epsilon}_{(n)}^{IS,el})$ is expressed by the Hooke's law. We obtain:

$$\text{tr}(\Delta \boldsymbol{\epsilon}_{(n)}^{STD}) = -\Delta p_{(n)}^{IS} / \chi + \text{tr}(\Delta \boldsymbol{\epsilon}_{(n)}^*) \quad (10)$$

where $\chi = E / (3(1 - 2\nu))$ is the elastic compressibility module, here taken at room temperature, and $\Delta p_{(n)}^{IS}$ is the pressure difference between states n and $n - 1$. Because the stress tensors should be the same for the two approaches (Eq. (8)b), the pressure difference is known from the STD-TEVP

simulations: $\Delta p_{(n)}^{IS} = \Delta p_{(n)}^{STD} = -(1/3)\text{tr}(\Delta \boldsymbol{\sigma}_{(n)}^{STD})$. This allows a direct determination of the spherical part of $\Delta \boldsymbol{\varepsilon}_{(n)}^*$, from the results of STD-TEVP simulations of states n and $n - 1$:

$$\text{tr}(\Delta \boldsymbol{\varepsilon}_{(n)}^*) = \text{tr}(\Delta \boldsymbol{\varepsilon}_{(n)}^{STD}) + (p_{(n)}^{STD} - p_{(n-1)}^{STD})/\chi \quad (11)$$

Taking now the deviatoric part of Eq. (7), we get:

$$\Delta \mathbf{e}_{(n)}^{STD} = \Delta \mathbf{e}_{(n)}^{IS,el} + \Delta \mathbf{e}_{(n)}^{IS,pl} + \Delta \mathbf{e}_{(n)}^* \quad (12)$$

where $\Delta \mathbf{e}_{(n)}^{STD}$, $\Delta \mathbf{e}_{(n)}^{IS,el}$, and $\Delta \mathbf{e}_{(n)}^*$ are the deviatoric parts of $\Delta \boldsymbol{\varepsilon}_{(n)}^{STD}$, $\Delta \boldsymbol{\varepsilon}_{(n)}^{IS,el}$, and $\Delta \boldsymbol{\varepsilon}_{(n)}^*$, respectively: $\Delta \mathbf{e}_{(n)}^{STD} = \Delta \boldsymbol{\varepsilon}_{(n)}^{STD} - (1/3)\text{tr}(\Delta \boldsymbol{\varepsilon}_{(n)}^{STD})\mathbf{I}$, with \mathbf{I} the identity tensor. The tensor $\Delta \mathbf{e}_{(n)}^{IS,el}$ is in turn expressed by the Hooke's law to obtain:

$$\Delta \mathbf{s}_{(n)}^{IS} = 2\mu \left[\Delta \mathbf{e}_{(n)}^{STD} - \Delta \mathbf{e}_{(n)}^{IS,pl} - \Delta \mathbf{e}_{(n)}^* \right] \quad (13)$$

where μ is the elastic shear modulus, and \mathbf{s} denotes the deviatoric part of the stress tensor: $\mathbf{s} = \boldsymbol{\sigma} + p\mathbf{I}$. Consider now the incremental plastic law between the two states $n - 1$ and n . Because the stress and strain tensors should be the same for the two approaches (Eq. (8)), and using the constitutive equations (Eqs. (2)-(3)), this leads to:

$$\left[1 + 2\mu\lambda(\Delta \bar{\varepsilon}_{(n)}^{IS}) \right] \mathbf{s}_{(n)}^{STD} = \mathbf{s}_{(n-1)}^{STD} + 2\mu \left[\Delta \mathbf{e}_{(n)}^{STD} - \Delta \mathbf{e}_{(n)}^* \right] \quad \text{with} \quad \bar{\sigma}_{(n)}^{IS} \leq \sigma_Y + R(\bar{\varepsilon}_{(n)}^{IS}) \quad (14)$$

It can be shown (details are not reported here, see [5]) that Eq. (14) is a non-linear equation to be solved for $\Delta \mathbf{e}_{(n)}^*$, by means, for instance, of a Newton-Raphson procedure. This being done, considering Eq. (11), the tensor $\Delta \boldsymbol{\varepsilon}_{(n)}^* = \Delta \mathbf{e}_{(n)}^* + (1/3)\text{tr}(\Delta \boldsymbol{\varepsilon}_{(n)}^*)\mathbf{I}$ is fully determined. Note that this direct determination of $\Delta \boldsymbol{\varepsilon}_{(n)}^*$ (based on the tensors $\boldsymbol{\varepsilon}_{(n)}$ and $\boldsymbol{\sigma}_{(n)}$ previously calculated by the standard TEVP simulation) can be achieved locally, *i.e.* in each finite element of the small-scale specimen. It does not require any additional global finite element resolution on the n -layer structure. This means that its resolution cost is negligible.

3.2. First validation on a small straight wall made of 8-layers

To validate the proposed inherent strain method, reference is made to the thermomechanical study of Biegler *et al.* of a straight wall made of stainless steel 316L by DED, using a back-and-forth single track deposition strategy [9]. The configuration composed of the first 8 layers is adopted for this first validation. The geometrical, material, and process parameters are documented in Table 1.

Table 1. Simulation data: material and process parameters, geometrical data.

	Properties	Values or reference
Material properties (stainless steel 316L)	Thermophysics	Kim [10]
	Thermomechanics	Muransky <i>et al.</i> [11]
Heat exchange	Initial temperature, T_0 [°C]	25
	Ambient temperature, T_{air} [°C]	25
	Convection coefficient, h_{conv} [W m ⁻² K ⁻¹]	35
	Emissivity, ε	0.6
	Stefan-Boltzmann constant, σ [W m ⁻² K ⁻⁴]	5.670374×10^{-8}
Process parameters (Biegler <i>et al.</i> [9])	Nominal laser power, P_L [W]	400
	Scan speed, v_L [mm s ⁻¹]	10
	Reflection coefficient, R	0.7
	Spot diameter, ϕ_L [mm]	0.6
	Inter-layer dwell time, t_{dwell} [s]	31
Part geometry (Biegler <i>et al.</i> [9])	Length, L [mm]	65
	Layer width, l_D [mm]	1.4
	Layer thickness, h_D [mm]	0.62
	Number of layers, N	30
	Total height, H [mm]	18.6
	Substrate, $L_\zeta \times l_\zeta \times h_\zeta$ [mm ³]	100 x 30 x 8

The average values of the 6 components of $\Delta \boldsymbol{\varepsilon}_{(n)}^*$ in each of the 8 layers are given in Table 2. Except for the first layer, they are globally similar. Shear components are quasi null ($<10^{-5}$), except for xz , the sign

of which changes due to the back-and-forth deposition. Regarding absolute values of diagonal terms, xx components are the largest, while yy and zz components are about twice as small.

Table 2. Average values of $\Delta\epsilon^*_{(n)}$ components in each of the 8 layers.

Layer n	Average values in layer					
	$\Delta\epsilon^*_{(n),xx}$	$\Delta\epsilon^*_{(n),yy}$	$\Delta\epsilon^*_{(n),zz}$	$\Delta\epsilon^*_{(n),xy}$	$\Delta\epsilon^*_{(n),xz}$	$\Delta\epsilon^*_{(n),yz}$
1	-0.0126	-0.0007	0.0127	0.	-0.0081	0.
2	-0.0144	0.0046	0.0093	0.	0.0079	0.
3	-0.0152	0.0058	0.0090	0.	-0.0079	0.
4	-0.0153	0.0063	0.0085	0.	0.0081	0.
5	-0.0151	0.0067	0.0079	0.	-0.0081	0.
6	-0.0148	0.0067	0.0074	0.	0.0089	0.
7	-0.0144	0.0067	0.0072	0.	-0.0089	0.
8	-0.0141	0.0068	0.0068	0.	0.0092	0.

To further evaluate the spatial distribution of $\Delta\epsilon^*_{(n)}$ the map of xx component is shown in Figure 2. In fact, in this representation, the 8 fields $\Delta\epsilon^*_{(n)}$ have been somewhat superimposed, depending on which layer each element belongs to. It is worth noting the heterogeneity in the first layers, but also near the two ends of the wall, where inherent strains clearly vary with height.

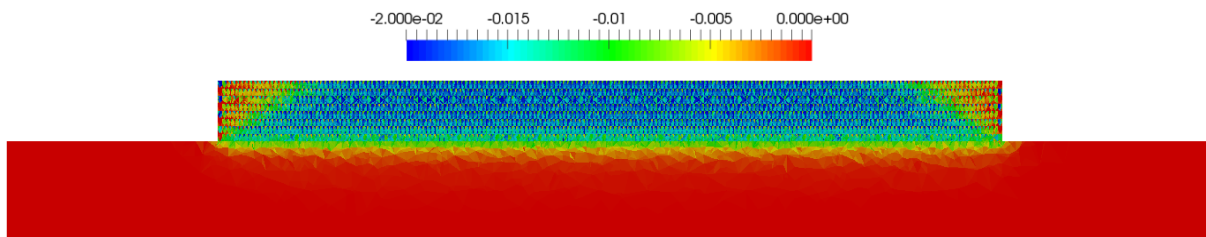


Figure 2. Map of $\Delta\epsilon^*_{xx}$ throughout the 8-layer wall and its substrate.

To validate the proposed IS method, the full tensor fields $\Delta\epsilon^*_{(n)}$ ($n = 1$ to 8) extracted as explained above, are applied for each layer addition, according to Eq. (7). Results are compared with the reference ones obtained by STD-TEVP. As shown in Figure 3, for distortion and stress along the deposition direction, the results obtained by the proposed IS method can hardly be distinguished from those obtained by STD-TEVP. This expresses that the proposed IS method quasi perfectly replicates the STD-TEVP simulation. However, this only validates i) the determination process of $\Delta\epsilon^*_{(n)}$, and ii) its use in the IS method. The strategy to apply the IS method to a large part is presented in the next Section.

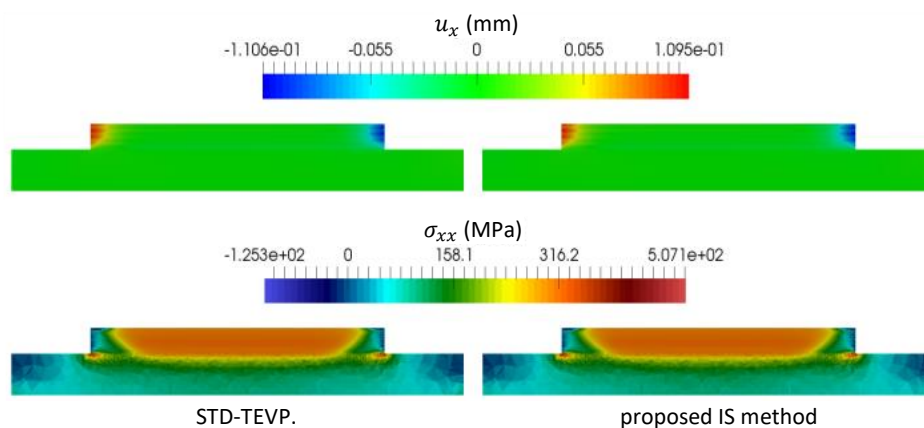


Figure 3. Validation of the proposed IS method on an 8-layer wall. Comparison of IS results (right) with reference STD-TEVP (left), for axial distortion and stress.

3.3. Application to the 30-layer straight wall: learning and transport strategy

Regarding now application of the IS method, especially for parts made of many layers, STD-TEVP simulations should be minimized. This needs to calculate approximate inherent strain fields in a simplified way, instead of calculating the exact $\Delta\epsilon^*_{(n)}$ for each layer addition as previously done. To

achieve this goal, it is chosen to determine the inherent strains on the first N_l layers – named learning layers – of the studied part. Following the identification of $\Delta\boldsymbol{\varepsilon}_{(n)}^*$, for $n = 1$ to N_l , it is then necessary to define how the inherent strains should be applied to model the addition of the rest of the layers ($n = N_l + 1$ to N). The method that is selected consists in transporting vertically the profile of inherent strains obtained from the learning layers. Taking care about the sign change for shear components due to back-and-forth deposition, we get, at location \mathbf{x} in layer $n > N_l$:

$$\begin{cases} \text{In layer } n \text{ such that } n - N_l \text{ is an even number: } \Delta\boldsymbol{\varepsilon}_{(n)}^*(\mathbf{x}) = \Delta\boldsymbol{\varepsilon}_{(N_l)}^*(\mathbf{x} - (n - N_l)h_D\mathbf{e}_z) \\ \text{In layer } n \text{ such that } n - N_l \text{ is an odd number: } \Delta\boldsymbol{\varepsilon}_{(n)}^*(\mathbf{x}) = \Delta\boldsymbol{\varepsilon}_{(N_l-1)}^*(\mathbf{x} - (n - N_l + 1)h_D\mathbf{e}_z) \end{cases} \quad (15)$$

where h_D is the layer thickness. Figure 4 illustrates the results of the proposed IS method, compared with STD-TEVP simulation, in the case of the 30-layer wall, using 4 learning layers. It can be seen that significant differences now appear. This result expresses the fact that the inherent strains identified in the learning layers do not reflect the inherent strains encountered in the upper layers. In fact, this result could have been anticipated, just looking at Figure 2. Therefore, the conclusion is that the IS method, definitely cannot replicate STD-TEVP.

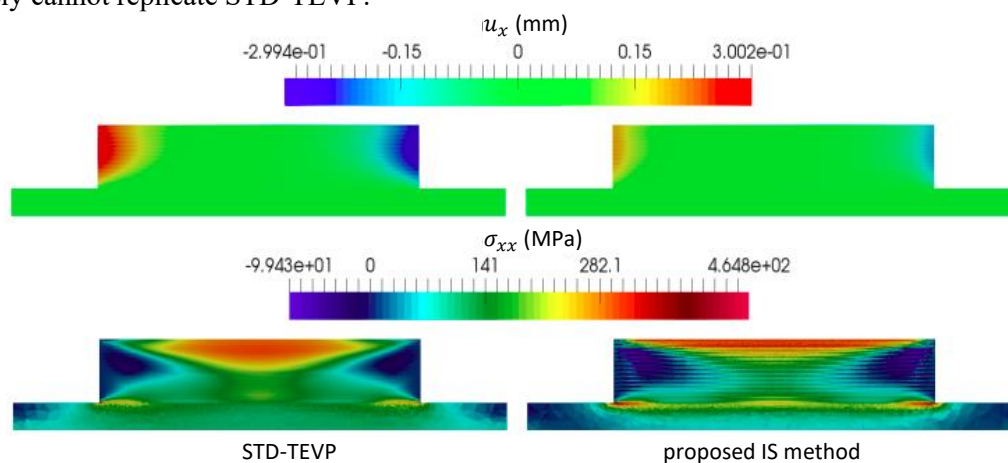


Figure 4. Application of the proposed IS method to the 30-layer wall, using 4 learning layers. Comparison with reference STD-TEVP for axial distortion and stress.

Regarding computer time, the IS method is 19 times faster than STD-TEVP. As a conclusion, the proposed new IS method was validated – by comparison with STD-TEVP – on a small-scale model, when using full-field inherent strains ($\Delta\boldsymbol{\varepsilon}_{(n)}^*$) in the different layers. However, the application of the IS method to the full 30-layer wall, using a few learning layers and transport of inherent strains, led to rather poor results, offering only a qualitative agreement with the reference STD-TEVP simulation. This result is disappointing, because the proposed IS method was especially designed to provide results as close as possible to the reference STD-TEVP. This was proved correct at small scale, but not at a larger scale. The reason for that is the heterogeneity of inherent strains on the learning layers, and, as a consequence, the impossibility to generate a field of inherent strains that would be appropriate on the whole construction. This is, in our opinion, a clear failure acknowledgement of the IS method. Finally, it appears relevant to develop an alternative approach of model reduction. In the following Section, we propose a new method, inspired by the IS method, but which is operated in a quite different way.

4. New method: the inherent strain rate method

The inherent strain rate method, ISR in short, consists of a linearization of the transient thermomechanical elastic-viscoplastic simulation (STD-TEVP). This linearization relies on the approximation of the generalized viscoplastic strain rate. This approximation is named "inherent strain rate" and is an input to the simulations (like the inherent strains in IS simulations). As such, this inherent strain rate (scalar) also requires an identification. But contrary to the IS method, identification is performed on-line, when simulating the studied part. The ISR approach is described hereafter.

4.1. Linearization of the thermo-elastic-viscoplastic constitutive equations

The constitutive equations for thermo-elastic-viscoplasticity are as follows:

$$\dot{\boldsymbol{\epsilon}} = \dot{\boldsymbol{\epsilon}}^{el} + \dot{\boldsymbol{\epsilon}}^{vp} + \dot{\boldsymbol{\epsilon}}^{th} \quad (16)$$

$$\dot{\boldsymbol{\epsilon}}^{el} = (\mathbf{D}^{el})^{-1} \dot{\boldsymbol{\sigma}} = \frac{1+\nu}{E} \dot{\boldsymbol{\sigma}} - \frac{\nu}{E} \text{tr}(\dot{\boldsymbol{\sigma}}) \mathbf{I} \quad (17)$$

$$\dot{\boldsymbol{\epsilon}}^{th} = \alpha \dot{T} \mathbf{I} \quad (18)$$

$$\dot{\boldsymbol{\epsilon}}^{vp} = \frac{3}{2\bar{\sigma}} \left[\frac{\bar{\sigma} - (\sigma_Y + R(\bar{\epsilon}))}{k} \right]_+^{1/m} \mathbf{s} \quad (19)$$

where the strain rate tensor $\dot{\boldsymbol{\epsilon}}$ is split into an elastic part, $\dot{\boldsymbol{\epsilon}}^{el}$, a viscoplastic part, $\dot{\boldsymbol{\epsilon}}^{vp}$, and a thermal part, $\dot{\boldsymbol{\epsilon}}^{th}$. α is the one-dimensional thermal dilation coefficient, $\dot{\boldsymbol{\sigma}}$ the time derivative of the stress tensor, k the viscoplastic consistency, m the strain rate sensitivity. The function $[x]_+$ is equal to 0 when x is negative and to x otherwise. From Eq. (19), when $\dot{\boldsymbol{\epsilon}}^{vp} \neq \mathbf{0}$, and calculating $\dot{\bar{\epsilon}} = \sqrt{(2/3)\dot{\boldsymbol{\epsilon}}^{vp} : \dot{\boldsymbol{\epsilon}}^{vp}}$, the following scalar relation can be easily obtained:

$$\bar{\sigma} = \sigma_Y + R(\bar{\epsilon}) + k \dot{\bar{\epsilon}}^m \quad (20)$$

Consequently, Eq. (19) can be straightforwardly rewritten:

$$\dot{\boldsymbol{\epsilon}}^{vp} = \frac{3\dot{\bar{\epsilon}}}{2\bar{\sigma}} \mathbf{s} \quad (21)$$

Non-linearity comes from the viscoplastic behavior law (Eq. (19) or (20)). The proposed linearization process consists in replacing the unknown equivalent strain rate $\dot{\bar{\epsilon}}$ by an a priori estimate, hereafter denoted $\dot{\bar{\epsilon}}^*$: the inherent strain rate. Proceeding in this way, we have at each time increment t :

$$\bar{\epsilon}(t) = \bar{\epsilon}(t - \Delta t) + \dot{\bar{\epsilon}}^* \Delta t \quad \text{and} \quad \bar{\sigma}(t) = \sigma_Y + R(\bar{\epsilon}(t)) + k \dot{\bar{\epsilon}}^{*m} \quad (22)$$

Therefore, the viscoplastic constitutive equation is linearized

$$\dot{\boldsymbol{\epsilon}}^{vp} = \frac{3\dot{\bar{\epsilon}}^*}{2\bar{\sigma}(\dot{\bar{\epsilon}}^*)} \mathbf{s} \quad (23)$$

Hence, the finite element resolution of the equilibrium equation $\nabla \cdot \boldsymbol{\sigma} = 0$, combined with constitutive equations (16)-(18) and (23) now requires a unique resolution, instead of an iterative solution process. The determination of the inherent strain rate $\dot{\bar{\epsilon}}^*$ and its application are detailed in the next sub-Sections.

4.2. Determination of inherent strain rates and ISR solution scheme

The inherent strain rate $\dot{\bar{\epsilon}}^*$ can be deduced from STD-TEVP calculation. When simulating with STD-TEVP, it is essential to remark that the most significant strain rates are found in the neighborhood of the material supply zone. This is evidenced in the left part of Figure 5.

From that, it is quite easy to elaborate simple rules (not detailed here) to define the shape of a simple domain – in red color in the right part of the figure – in which a uniform inherent strain rate $\dot{\bar{\epsilon}}^*$ will be defined as the volume average of the most significant strain rates.

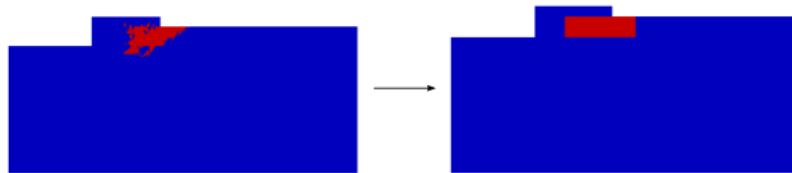


Figure 5. Left: during STD-TEVP simulation of the deposition of the third layer, the red zone encompasses elements showing the top 10% highest strain rates. Right: the red zone indicates the domain in which a uniform inherent strain rate $\dot{\bar{\epsilon}}^*$ is to be applied.

The strategy to simulate the construction process consists then in a succession of linearized resolutions of the elastic-viscoplastic deformation of the structure, interrupted by some full (non-linear) STD-TEVP resolutions to update the value of the inherent strain rate, and its application domain. In practice, the use of the two solvers is organized as shown in Figure 6. The STD-TEVP resolution is used at each layer for the very first time steps at deposition start, and for a very few time increments at the transition between deposition end and dwell-time. All other time steps are solved with the ISR method. Only the first two layers are treated differently, STD-TEVP being used all along layer deposition.

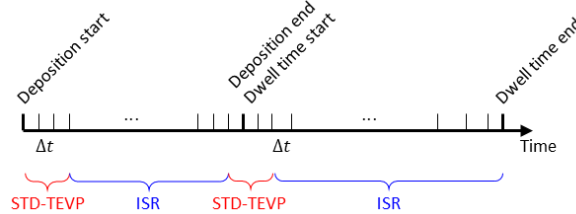


Figure 6. Organisation of the ISR solution method to simulate the deposition of a layer, and the subsequent inter-layer dwell time. STD-TEVP stands for the use of the non-linear resolution, while ISR stands for the use of the linearized elastic-viscoplastic resolution.

4.3. Application of ISR method to the 30-layer wall

Apart from the larger number of layers, geometrical data, process parameters and material properties are identical to those given in Section 3.2. Figure 7 shows the comparison, in terms of predicted distortion and stress fields, between ISR and STD-TEVP. The difference between displacement or stress components is not perceptible (relative difference less than 1%).

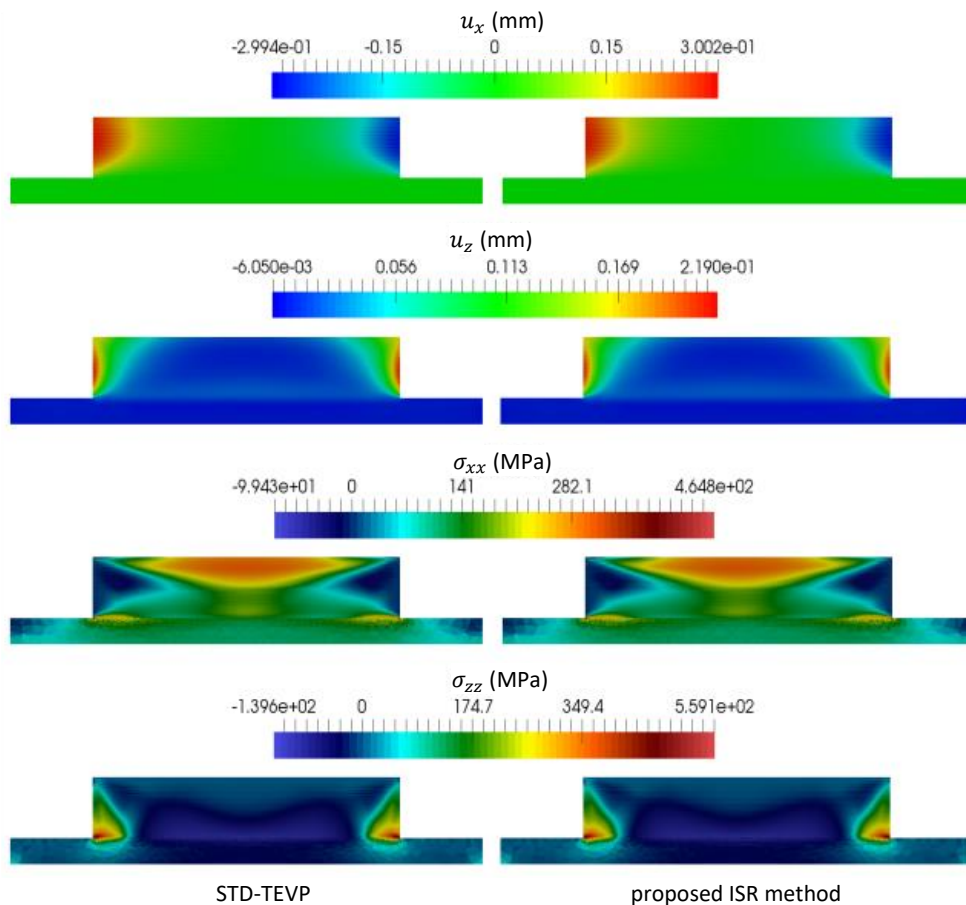


Figure 7. Application of ISR method to the 30-layer wall. Distortion and stress fields (x and z components) after complete cooling.

Regarding computation time, the ISR method shows a speed-up ratio of 5.2 with respect to STD-TEVP on the studied configuration. This is certainly lower than for the IS method, but the accuracy of the results is invaluablely better. Also, it can be anticipated that this speed-up ratio could be higher on more complex simulation cases and could be improved by minimizing the number of STD-TEVP resolutions.

5. Conclusion

The lack of fidelity of the IS method with respect to a reference STD-TEVP numerical simulation has been evidenced. This fundamental weakness is due to the fact that the learning process made on a small-scale test part (possibly on a first few layers of the studied part) fails to be representative of the inherent strains undergone by the deposited material during deposition of the upper layers of the construction. Conversely, the new ISR method – based on a linearization process of realistic elastic-viscoplastic constitutive equations, and equipped with an efficient on-line learning process – perfectly replicates the reference calculations. Although less computer efficient, in its current state of development, than the IS method, the ISR method is very promising.

6. References

- [1] Ueda Y, Fukuda K, Nakacho K, Endo S 1975 *J. Soc. Naval Architects of Japan* **1975** 499
- [2] Keller N, Ploshikhin V 2014 *Proc. 25th Annual International Solid Freeform Fabrication Symposium, U. Texas, Austin*, 1229
- [3] Alvarez P, Ecenarro J, Setien I, San Sebastian M, Echeverria A, Eciolaza L 2016 *Int. J. Eng. Research and Science* **2** 39
- [4] Liang X, Cheng L, Chen Q, Yang Q, To AC 2018 *Additive Manufacturing* **23** 471
- [5] Keumo Tematio J 2022 *PhD Thesis*, PSL University, Mines Paris
- [6] Setien I, Chiumenti M, van der Veen S, San Sebastian M, Garciandía F, Echeverría A 2019 *Comput. and Math. with Appl.* **78** 2282
- [7] Siewert M, Neugebauer F, Epp J, Ploshikhin V 2019 *Comput. and Math. with Appl.* **78** 2407
- [8] Duan C, Cao X, Luo X 2021 *IOP Conf. Series: Earth and Environmental Science* **714** 032032
- [9] Biegler M, Graf B, Rethmeier M 2018 *Additive Manufacturing* **20** 101
- [10] Kim CS 1979 *Technical Report Argonne National Laboratory*, Ill., USA
- [11] Muransky O, Smith MC, Bendeich PJ, Edwards L 2011 *Comp. Mater. Sci.* **50** 2203